

Liquid crystal trimers containing tertiary benzanilide groups.

STRACHAN, G.J., MAJEWSKA, M.M., CRUICKSHANK, E., POCIECHA, D.,
GORECKA, E., STOREY, J.M. and CORRIE, T.I.

2025

© The Royal Society of Chemistry 2025.

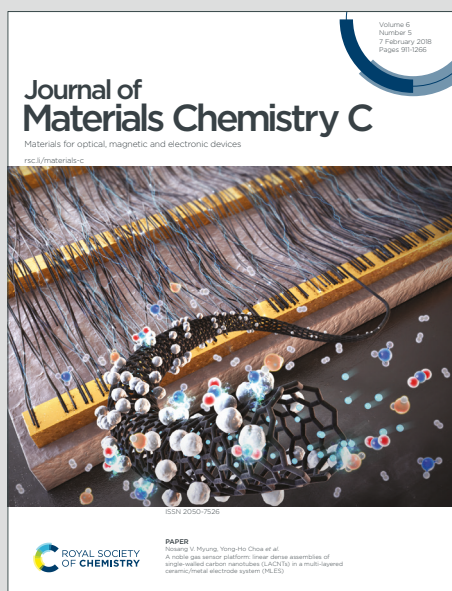
Supplementary materials are appended after the main text of this document.

Journal of Materials Chemistry C

Materials for optical, magnetic and electronic devices

Accepted Manuscript

This article can be cited before page numbers have been issued, to do this please use: G. J. Strachan, M. Majewska, E. Cruickshank, D. Pocięcha, E. Gorecka, J. M. D. Storey and C. T. Imrie, *J. Mater. Chem. C*, 2025, DOI: 10.1039/D5TC01532D.



This is an Accepted Manuscript, which has been through the Royal Society of Chemistry peer review process and has been accepted for publication.

Accepted Manuscripts are published online shortly after acceptance, before technical editing, formatting and proof reading. Using this free service, authors can make their results available to the community, in citable form, before we publish the edited article. We will replace this Accepted Manuscript with the edited and formatted Advance Article as soon as it is available.

You can find more information about Accepted Manuscripts in the [Information for Authors](#).

Please note that technical editing may introduce minor changes to the text and/or graphics, which may alter content. The journal's standard [Terms & Conditions](#) and the [Ethical guidelines](#) still apply. In no event shall the Royal Society of Chemistry be held responsible for any errors or omissions in this Accepted Manuscript or any consequences arising from the use of any information it contains.

Liquid crystal trimers containing tertiary benzanilide groups.

View Article Online
DOI: 10.1039/D5TC01532D

Grant J. Strachan,^{a†} Magdalena M. Majewska,^b Ewan Cruickshank,^{a‡} Damian Pocięcha,^b Ewa Gorecka,^b John M.D. Storey,^a Corrie T. Imrie.^{a*}

*Author for correspondence: gj.strachan@outlook.com

^a Department of Chemistry, School of Natural and Computing Sciences, University of Aberdeen, Meston Building, Aberdeen, AB24 3UE, UK

^b Faculty of Chemistry, University of Warsaw, ul. Pasteura 1, 02-093 Warsaw, Poland

[†]Current address: Faculty of Chemistry, University of Warsaw, ul. Pasteura 1, 02-093 Warsaw, Poland

[‡]Current address: School of Pharmacy, Applied Sciences and Public Health, Robert Gordon University, Aberdeen, AB10 7GJ, UK

*Deceased 14th January 2025

Abstract

The rational design of new liquid crystal materials relies on an understanding of the relationship between molecular structure and the formation of liquid crystalline phases. The development of new materials can benefit from the use of a wide range of functional groups, but some groups prove challenging to combine with liquid crystallinity. Tertiary benzanilide groups are a clear example of this, as their strong conformational preferences disrupt liquid crystallinity when included in typical liquid crystalline structures. This means that it has not been possible to harness the molecular design possibilities offered by amide *N*-substitution. However, designing flexible structures to accommodate the conformation of tertiary benzanilides has allowed us to synthesise a variety of liquid crystal trimers forming nematic and smectic phases, and investigate the effect of lateral and *N*-substitution on their phase behaviour. Trimers with large (benzyl and decyl) *N*-substituents favour the formation of an orthogonal smectic (SmA) phase and demonstrate unusual and highly pronounced contraction of the smectic layer spacing on cooling, illustrating the non-conventional properties enabled by the unusual structures of these amide-based liquid crystals.

Introduction

The study of liquid crystals (LCs) with unconventional molecular shapes (Figure 1) which do not fit neatly into the traditional groups of calamitic (rod-like, with one long and two shorter molecular axes) or discotic (disc-shaped, with one short and two longer molecular axes) materials has become a rapidly expanding area of research. This has led to the discoveries of the 'banana' phases¹ formed by rigid bent-core mesogens and the twist-bend nematic (N_{TB})^{2,3} and smectic (SmC_{TB})⁴ phases formed by bent-shaped molecules. The search for new liquid crystalline architectures is driven by two main objectives. Firstly, it allows researchers to develop a fundamental understanding of the structure-property relationships driving the formation of LC phases. This in turn facilitates the fine-tuning of the phase behaviour of LCs by tailoring their molecular structure in a rational manner and opens new design approaches to LC materials through the inclusion of different chemical functionalities. Secondly, the expansion of our knowledge base will allow for the unique properties of LCs, such as



spontaneous self-assembly or ease of alignment, to be harnessed in the development of functional materials.^{5,6}

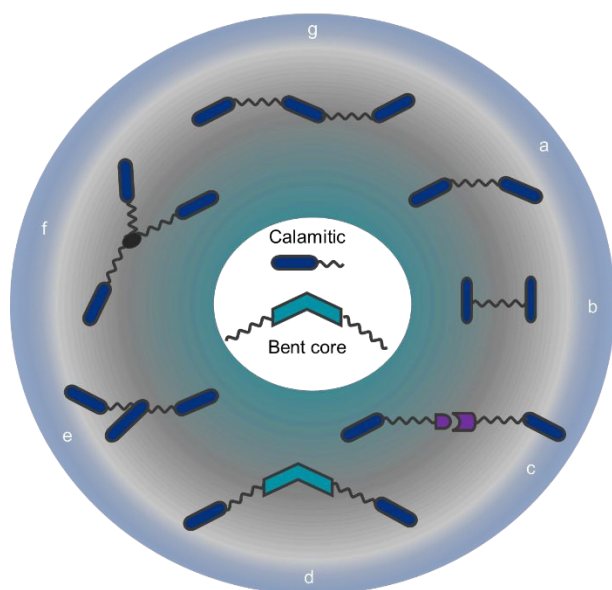


Figure 1: Sketches of different mesogenic architectures: conventional low molar mass calamitic and bent core⁷ mesogens (centre). a: linearly-linked bent dimer,⁸ b: H-shaped dimer,⁹ c: hydrogen-bonded LC,¹⁰ d: bent-core trimer,¹¹ e: λ -shaped trimer,¹² f: tripodal trimer,¹³ g: linearly-linked trimer.¹⁴

One such new and underexplored fragment is the benzanilide moiety, which consists of an amide group linking two benzene rings. In principle this can be used in a similar manner to phenyl benzoate or benzyldineaniline groups which have been used extensively in the design of new mesogens. However, the benzanilide group has been only sparingly used in the development of low molar mass LCs. The hydrogen bonding present between secondary benzanilides has been harnessed to promote the formation of lamellar phases,^{15–17} whereas tertiary benzanilides (with an additional functionality at the amide nitrogen) have frequently proved to be non-mesogenic. We have recently shown that this is due to the unconventional shape of mesogens containing tertiary benzanilides, driven by the strong preference for the *E* amide conformation seen in these materials (Figure 2).¹⁸ Earlier attempts to incorporate tertiary benzanilides into LC architectures, such as rigid bent cores or in flexible dimers, were not designed to accommodate this conformation and as a result, tertiary benzanilide-based materials have shown very limited liquid crystalline behaviour compared to their secondary benzanilide counterparts. We proposed that the increased flexibility of a trimeric LC structure (Figure 1) could more readily accommodate the *E* amide conformation of tertiary benzanilides and allow for the development of a new class of mesogenic materials based on the benzanilide group.



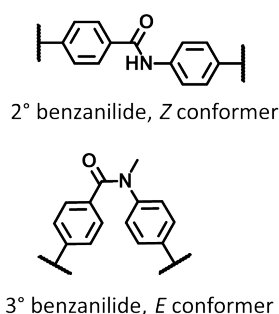


Figure 2: The *Z* and *E* conformers adopted by secondary and tertiary benzanilides.

In the first part of this work, we investigated the phase behaviour and the effect of structural modifications in a series of six tertiary benzanilides with *N*-methyl substituents. In the second part, we examine the effect of introducing larger substituents on the amide nitrogen, to demonstrate the use of this group as an additional tool for the structural modification of LC materials. The structures of the trimers are given in Table 1, and the general structure consists of two terminal mesogenic units linked to the central benzanilide unit by flexible spacers. To investigate the effects of structural modification on phase behaviour in these trimers, changes were made to the length of the spacers, the number and position of lateral methyl substituents, and the nature of the substituent on the amide nitrogen.

Methods

The syntheses of the trimers reported here were carried out according to literature methods, and full experimental details and structural characterisation data are given in the SI.

The phase behaviour of the materials was studied using differential scanning calorimetry (DSC) with a Mettler Toledo DSC3 differential scanning calorimeter equipped with a TSO 801RO sample robot and calibrated with indium and zinc standards. The heating and cooling rates were 10 K min⁻¹ and the transition temperatures and their associated enthalpy changes were extracted from heating traces unless otherwise noted.

Optical textures were used to identify the liquid crystal phases, and these were observed using an Olympus BH2 polarising optical microscope equipped with a Linkam TMS 92 heating stage. Optical birefringence was measured with a setup based on a photoelastic modulator (PEM-90, Hinds) working at a modulation frequency $f = 50$ kHz; a halogen lamp (Hamamatsu LC8) equipped with narrow bandpass filters was used as a light source. The signal from a photodiode (FLC Electronics PIN-20) was deconvoluted with a lock-in amplifier (EG&G 7265) into 1 *f* and 2 *f* components to yield a retardation induced by the sample. Knowing the sample thickness, the retardation was recalculated into optical birefringence. Samples were prepared in 3-micron-thick cells with planar anchoring. The alignment quality was checked prior to measurement by inspection under the polarised optical microscope. AFM measurements were performed using a Bruker Dimension Icon Microscope working in tapping or scan assist mode and cantilevers with elastic constant of 0.4 N/m were applied. X-ray diffraction measurements were carried out using a Bruker D8 GADDS system with CuK α radiation, Goebel mirror monochromator, point beam collimator, and VANTEC2000 area detector. SAXS measurements were performed on a Bruker Nanostar system using CuK α radiation and patterns were collected with an area detector VANTEC2000.

Results

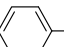
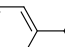
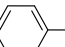
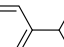


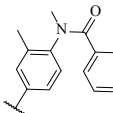
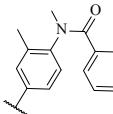
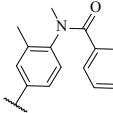
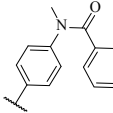
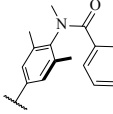
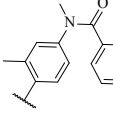
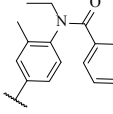
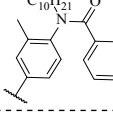
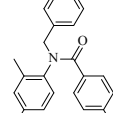
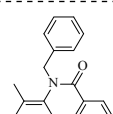
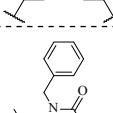
The ^1H NMR spectra of the trimers are consistent with the expected *E* amide conformation and this was confirmed by 2D NOESY NMR spectroscopy for trimers **1** and **5**. NOESY experiments measure through-space correlations, showing atoms that are close together, rather than the through-bond correlations measured in most NMR experiments. The two possible amide conformations, *E* and *Z*, would each show a different set of correlations in the NOESY spectra, and this can be used to identify their conformation. The spectra recorded for both trimers showed only the correlations consistent with the *E* conformation, and these are shown in Figure S1. It is important to note that all the NMR studies were carried out in solution and therefore do not directly confirm the structure of the materials in a condensed state. All the trimers formed enantiotropic liquid crystal phases, and the transition temperatures and associated entropy changes are given in Table 1.

View Article Online
DOI: 10.1039/D5TC01532D



Table 1: Transition temperatures and the associated scaled entropy changes for trimers reported here. ‡Denotes values taken from POM. †Taken from initial heating DSC trace. *The entropy changes could not be determined due to peak overlap in the DSC trace.

NC---(CH2)nO-**Core**-O(H2C)n---CN

	Core	n		Melt	SmA-N	N-I
1		6	T / °C	102	132‡	182
			ΔS / R	2.58		0.10
2		8	T / °C	106	148	178
			ΔS / R	2.70	0.04	0.17
3		10	T / °C	100	148	178
			ΔS / R	2.35	0.02	0.13
4		6	T / °C	92		201
			ΔS / R	2.83		0.16
5		6	T / °C	98	130	175
			ΔS / R	1.68	0.06	0.11
6		6	T / °C	97	123‡	180
			ΔS / R	3.01		0.14
7		6	T / °C	100	123	154
			ΔS / R	2.81	0.03	0.08
8		6	T / °C	108	131	143
			ΔS / R	2.91	0.08	0.09
9		6	T / °C	111	133	147
			ΔS / R	3.62	0.11	0.08
10		8	T / °C	117	143	148
			ΔS / R	3.27	0.24	0.08
11		10	T / °C	118	144*	147*
			ΔS / R	2.87		



The *N*-methylated compounds

All 6 compounds with an *N*-methyl substituent (**1** - **6** in Table 1) formed enantiotropic nematic phases. These were identified by the observation of schlieren textures with 2- and 4-point brush defects using POM and confirmed by X-ray diffraction measurements which revealed only short-range order, see representative optical texture and X-ray diffraction pattern for **1** in Figure 3. In addition, all trimers with lateral methyl substituents on the anilide ring, **1-3**, **5**, and **6**, formed a second enantiotropic LC phase. X-ray diffraction patterns for this phase contained two main signals: a diffuse signal in the wide-angle region, and a sharp signal in the small angle region, indicating a liquid-like smectic phase. A third, weaker diffuse signal is seen in the small angle region. POM textures obtained with the sample sandwiched between untreated glass slides showed fan-like textures, which sheared to give homeotropic alignment. Based on this, the phase was identified as a SmA phase, and a representative example of the textures and X-ray patterns are shown in Figure 3. Measurements of the temperature dependence of the optical birefringence revealed an increase in Δn at the N-SmA transition, as would be expected due to the increasing molecular order (Figure 3). Increasing the length of the flexible spacers from 6 carbons in **1**, to eight and ten carbons in **2** and **3**, respectively, had essentially no effect on T_{NI} . The increased spacer length in **2** stabilised the SmA phase, with T_{SmAN} increasing by 16 K, but further increasing the spacer length in **3** had no effect. This somewhat surprising observation highlights the unusual shape of these mesogens arising from the *E* conformation of the central benzanilide group. For comparison, we have previously reported the phase behaviour of the corresponding secondary benzanilides, and for these materials increasing the spacer length not only produced a notable change in transition temperatures, but to different LC phases being formed.¹⁹

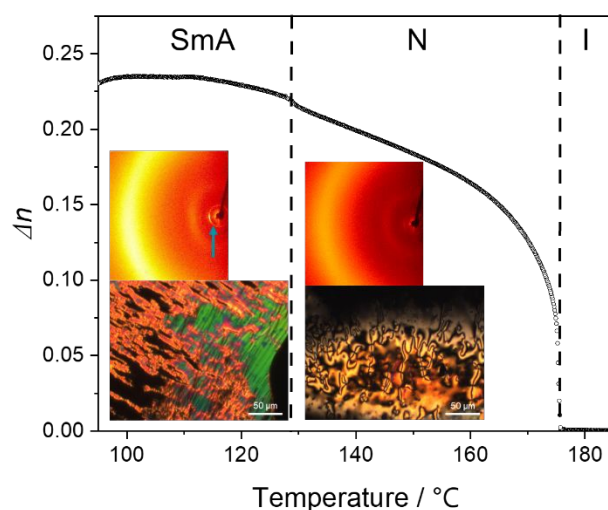


Figure 3: The temperature dependence of the optical birefringence of **1**. Inset left: POM texture of **1** in the SmA phase at 100 °C between untreated glass slides and the X-ray diffraction pattern of the SmA phase at 125 °C. The blue arrow highlights the sharp small-angle signal corresponding to the main layer spacing. Inset right: POM texture of **1** in the N phase at 134 °C between untreated glass slides and X-ray diffraction pattern of the N phase at 140 °C.

To understand this unusual behaviour, it is necessary to consider the arrangement of the molecules within the SmA phase. Based on the X-ray diffraction patterns recorded in the SmA phase for compound **1**, a proposed packing arrangement is given in Figure 4. The sharp signal



seen in the small angle region corresponds to the bilayer arrangement of the bent-shaped molecules, while the weaker, diffuse small angle signal is believed to arise from local short-range ordering of the cyanoterphenyl units and can also be seen in the diffraction pattern recorded in the nematic phase. In such an arrangement, the overall bent structure of the molecules counteracts, to some degree, the increase in the length of the spacers, leading to an increase in the layer spacing without a dramatic change in the transition temperatures or phase behaviour. X-ray measurements do show a shift in the layer spacing (Table 2) from 42 Å for **1**, to 46 Å and 47 Å for **2** and **3**, respectively. This trend is consistent with the proposed packing arrangement in Figure 4, as the increase in layer spacing is less than the increase in length expected from the additional methylene units if the molecules were in an elongated linear conformation. In addition, the very small changes in $\Delta S/R$ (Table 1) seen for the N-SmA transition are consistent with the highly bent trimer structure arising from the *E*-amide conformation.

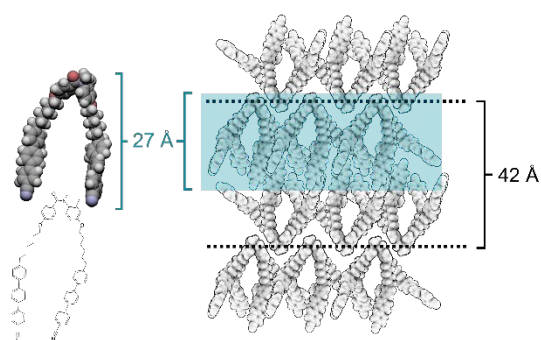


Figure 4: Left: structure and space filling model of trimer **1**. Right: Sketch of the proposed packing of **1** in the SmA phase. The shaded area shows the approximate length of the trimer in the bent conformation.

Table 2: Layer spacings determined from X-ray diffraction measurements for trimers **1-3**, and **7-11**.

Trimer	Sharp small angle signal / Å	Diffuse small angle signal / Å
1	42	15
2	46	16
3	47	17
7	46	15
8	54	16
9	47 ^a	17 ^a
10	50	16
11	53	17

^aMeasured using SAXS

An unexpected textural change was observed for samples sandwiched between untreated glass slides at temperatures slightly above the N-SmA transition for compounds **1-3**. A striped texture was seen to develop in thin regions of the sample (Figure 5), and its evolution over the transition from the N to SmA phase is shown in Figure 6. The texture in the N phase contains two- and four-brush defects confirming the assignment. On cooling filaments appear to develop that are crossed by fine lines, which become more apparent on cooling. These appear not to be perfectly periodic and thus not associated with a helical structure but instead presumably are indicative of an increase in order at the approach to the SmA phase, perhaps reflecting the strongly biaxial structure of these molecules. The precise physical significance



of these stripes is not clear, but they appear to resemble textures reported for samples of 8CB or 8OCB prepared under hybrid alignment conditions,^{20–22} although the samples reported here were simply prepared between two untreated glasses. The observation of such stripes, or undulations, has been interpreted in terms of diverging elastic constants at the N-SmA transition, and that may also apply to the materials reported here, although further study is required to fully understand these observations.

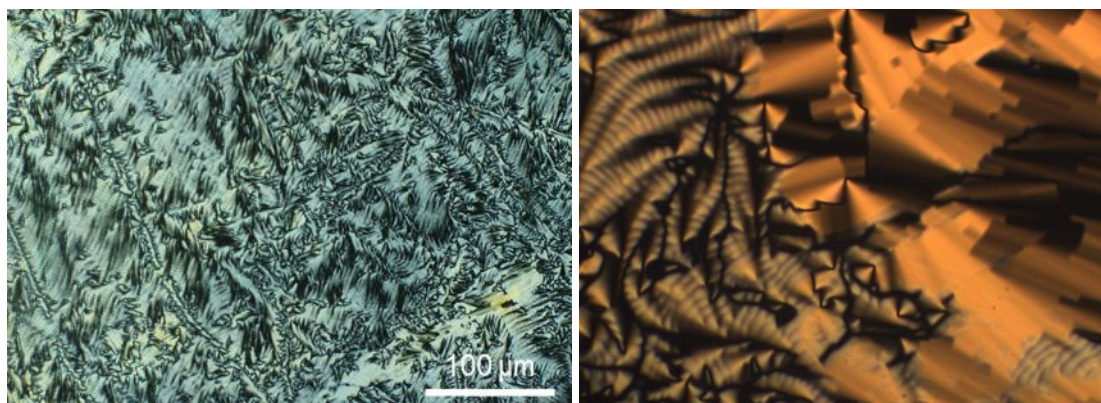


Figure 5: POM texture of **1** at (left) 132 °C and (right) 130 °C on cooling, showing stripes.

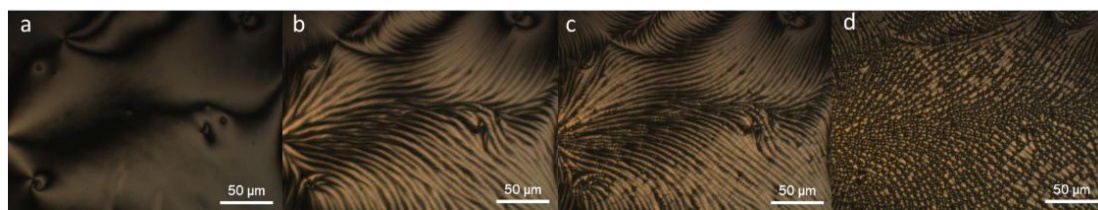


Figure 6: The evolution of the POM texture seen for **3** on cooling from the nematic to smectic A phase: a) the schlieren texture in the nematic phase at 149 °C; b) the formation of stripes across the nematic texture at 148 °C; c) the break of the stripes on further cooling to 146 °C; d) the texture observed in the SmA phase at 143 °C.

The effect of lateral substitution

Trimers **4**, **5**, and **6** are variations of structure **1** with differing lateral methyl substitution on the anilide ring and representative POM textures for these trimers are given in Figure 7. Trimer **4** has no lateral substituents, trimer **5** has two *ortho* substituents, and **6** has a single methyl substituent in the *meta* position. The greatest difference is seen for the unsubstituted compound **4**, for which T_{NI} is 20 K higher than **1**, but no smectic behaviour is seen. In contrast, the transition temperatures of the di-*ortho*-substituted **5** are essentially the same as **1**, while moving the methyl from the *ortho* to the *meta* position in trimer **6** leads to a decrease of ~10 K in T_{SmAN} . Comparing these materials, it becomes apparent that the presence of at least one lateral substituent close to the amide group is required to promote the SmA phase and removing the lateral substituents leads to a loss of smectic behaviour. This suggests that *ortho* substituents help to fill space within the bilayer structure proposed in Figure 4, and moving the substituent to the *meta* position means this space filling is less efficient.



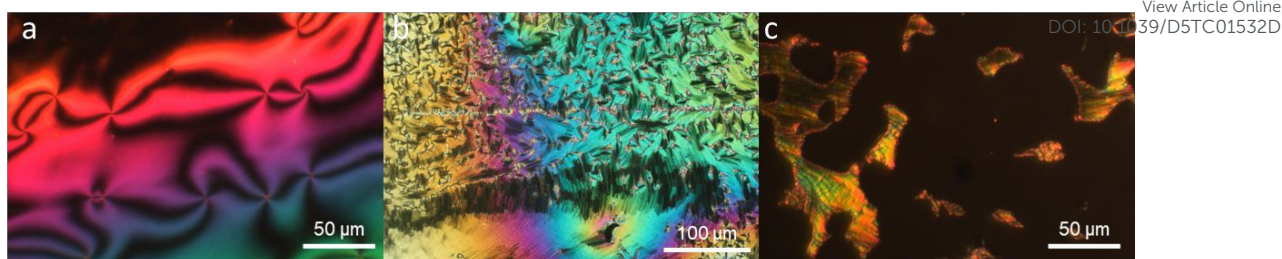


Figure 7: a) The schlieren texture of **4** in the nematic phase at 115 °C, b) the fan-like texture of **5** in the SmA phase at 120 °C, and c) the homeotropic texture of **6** in the SmA phase at 102 °C.

Larger *N*-substituents

The effect of increasing the length of the alkyl *N*-substituents was studied in compounds **7** and **8**, the ethyl and decyl substituted analogues, respectively, of the methylated compound **1**. Both compounds showed the same phase sequence as **1**, forming enantiotropic N and SmA phases, and POM textures obtained for these phases, Figure 8, show optically extinct regions consistent with the assignment of an SmA phase. The nematic phase was destabilised by the larger *N*-substituents, with T_{NI} decreasing by 28 K for **7** and 39 K for **8** compared to that of **1**. This may be attributed to the disruption of the interactions between the mesogenic units as the *N*-substituent becomes larger. However, the stability of the SmA phase for the *N*-ethyl substituted **7** was not affected as strongly – with a decrease of only 9 K seen in T_{SmAN} compared to **1**. Surprisingly, increasing the length of the *N*-substituent further in the decyl substituted **8** led to an increase in T_{SmAN} compared to **7**, such that it is essentially the same as that of the methyl substituted **1**.

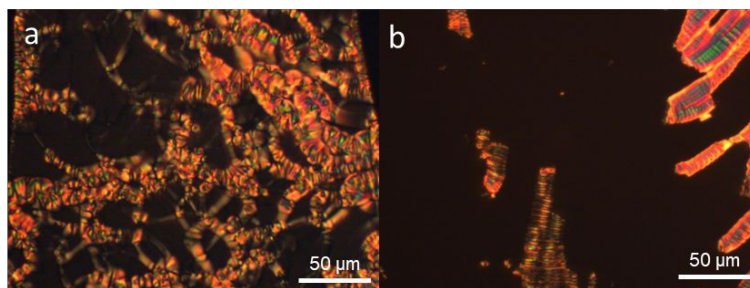


Figure 8: POM textures observed in the SmA phase on untreated glass for a) **7** (109 °C) and b) **8** (128 °C).

The final three compounds, **9**, **10**, and **11**, are the *N*-benzyl analogues of **1**, **2**, and **3**, with six-, eight- and ten-carbon spacers, respectively. Again, these materials all formed enantiotropic nematic and SmA phases. Compared to their *N*-methylated counterparts, the introduction of the larger benzyl substituent again destabilised the nematic phase, with decreases in T_{NI} of ~30 K. As was seen for trimers **1-3**, increasing the spacer lengths in **9-11** had no appreciable effect on T_{NI} . In contrast to their clearing temperatures, T_{SmAN} for the *N*-benzylated materials were very similar to those of their *N*-methylated counterparts. This, somewhat counterintuitively, indicates that the larger *N*-benzyl group is more easily accommodated in the SmA phase, than in the nematic phase. However, as was discussed for trimers **4-6**, it may be that additional substitution around the amide group helps to fill space within the bilayer packing of the SmA phase, and substitution at the nitrogen (the apex of the molecule) may be reasonably easily accommodated within the bilayer structure. Interestingly, measurements of the temperature dependence of the layer spacing showed a marked contraction across the



SmA phase on cooling for the materials with larger (decyl or benzyl) *N*-substituents, and this is shown in Figure 9 for compound **11** and Figure S2 for **2**, **8-11**. In general, smectic A phases would be expected to exhibit negative thermal expansion, such that their layer spacing increases on cooling.^{23–25} Decreasing layer spacing, as reported here, would typically be associated with the formation of a tilted smectic phase, e.g. SmC. However, this is not the case for SmA phases with partial bilayer structure (interdigitation), such as that formed by the widely-studied smectogen 8CB,²⁶ and this observation supports our suggested packing arrangement sketched in Figure 4. While this may explain the trends we report in the layer spacing changes on cooling, the magnitude of the decreases measured for the *N*-benzyl trimers, ca. 3 Å, are an order of magnitude larger than those reported in the nCB series, ca. 0.3 Å.²⁷

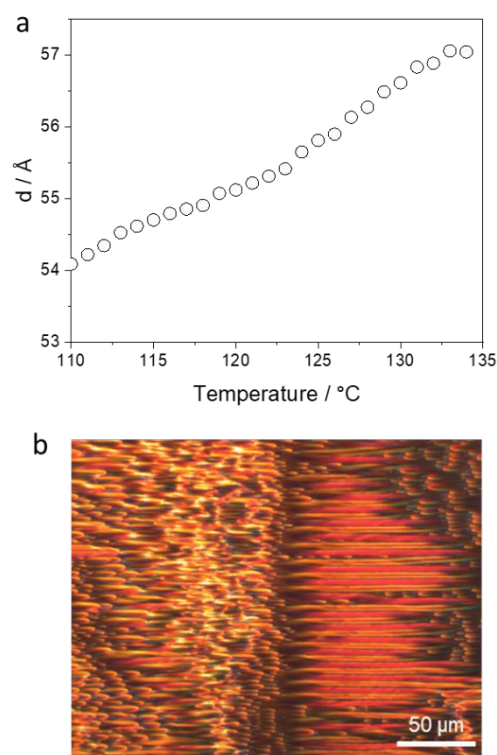


Figure 9: (a) The temperature dependence of the layer spacing of trimer **11** in the SmA phase. (b): the striped and parabolic POM texture observed in the SmA phase at 129 °C in a cell treated for planar alignment.

It was also observed that materials with larger *N*-substituents (**7-11**) had a pronounced tendency to produce a mix of focal conic defects and apparent striped textures in planar aligned cells studied using POM (Figure 9b). The appearance of striped textures appears to result from the decrease in layer thickness on cooling these trimers, and the accompanying distortion of the smectic layers. The observation of such striped textures in an SmA phase has been reported previously.²⁸ The materials studied, II/6 and 9ZBL, had thermal expansion coefficients of $k_t = -0.8 \times 10^{-3} \text{ nm K}^{-1}$ and $k_t = -1.8 \times 10^{-3} \text{ nm K}^{-1}$, respectively. These negative coefficients correspond to an increase in the layer spacing on cooling and was considered typical for smectic A phases. From the X-ray measurements of layer spacing for the trimers reported here, we have calculated the thermal expansion coefficients for the compounds with the largest *N*-substituents; **8-11**, and the *N*-methylated trimer **2** for comparison, and these are listed in Table 3. Trimer **2**, with the smallest, *N*-methyl, substituent, has k_t of very similar



magnitude to that reported for 9ZBL, but of the opposite sign. This is due to the different packing arrangements present in the SmA phases of the two materials, as discussed previously, with the positive k_t of trimer **2** relating to the bilayer packing arrangement in the SmA phase. However, increasing the size of the *N*-substituent in trimer **8** led to a tripling of k_t , and introducing an *N*-benzyl substituent in **9**, **10**, and **11**, produced an even greater increase. These unusually large values of k_t correspond to very pronounced layer contraction on cooling the SmA phase, on a scale that would normally be expected in tilted, SmC phases. This highlights the unusual properties of these highly bent trimers, introduced through the central tertiary amide unit.

Table 3: Thermal expansion coefficients, k_t , calculated from X-ray measurements.

trimer	<i>N</i> -substituent	$k_t / \times 10^{-3} \text{ nm K}^{-1}$
2	Methyl	1.8
8	Decyl	5.6
9	Benzyl	11
10	Benzyl	10
11	Benzyl	12

AFM studies of trimers **9** and **11** in split cells with planar alignment layer showed clear focal conic structures, (Figure 10), which arise from the interplay of molecular ordering and the layered nature of the smectic A phase. The confocal ellipses observed in the AFM pictures are a direct result of the SmA phase requirement for equidistant layers.

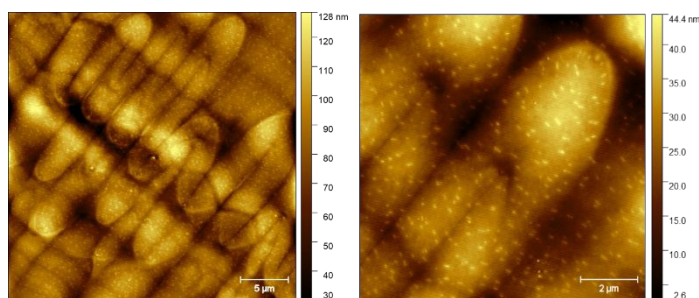


Figure 10: AFM images for trimers **9** and **11** showing focal conics of the SmA phase.

Comparing the behaviour of bent and linear trimers containing tertiary or secondary benzanilides

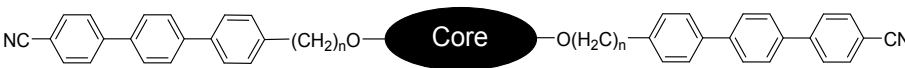
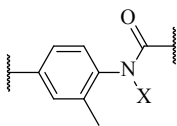
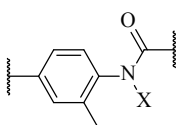
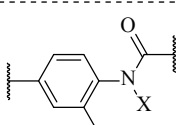
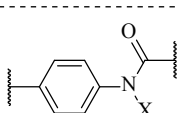
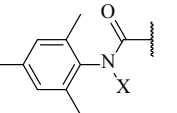
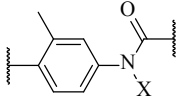
The influence of the molecular shape on phase behaviour can be clearly seen when the phase behaviour of these trimers are compared to their corresponding secondary amides. These are given in Table 4, and the trimers are grouped according to their base structures, with either *N*-*H*, *N*-*CH*₃ or *N*-*Bn* groups. All the trimers form a nematic phase, and the clearing temperatures of the secondary amides (*N*-*H*) are consistently much higher than comparable tertiary amide (*N*-*CH*₃), generally by around 100 K. While the loss of hydrogen bonding on *N*-alkylation would be expected to decrease T_{NI} , this would not be expected to have such a large effect. However, the highly bent structure introduced by the *E* amide conformation would be less compatible with the nematic phase than the more linear structure adopted by the secondary amide trimers.

The secondary amides also show phase sequences typical for linearly linked trimers with odd-membered spacers; the C10 homologue forms the twist-bend nematic phase, and the C6 and



C8 homologues form triply intercalated smectic phases, with layer spacings corresponding to approximately one third of their molecular length. All three trimers with C8 spacers formed a smectic A phase, and this allows the layer spacings to be directly compared: in the secondary amide trimer, this was 19 Å, corresponding to one-third of the molecular length of the trimer in an extended, linear conformation with the Z-amide conformer. This represents a triply intercalated packing arrangement. In contrast, the tertiary amide analogues reported here had a layer spacing of 46 Å (*N-CH₃*) and 50 Å (*N-Bn*), which suggests a bilayer structure of the SmA phase, as sketched in Figure 4. This change in the way the trimers pack within the SmA phase highlights the very different molecular shapes of the secondary and tertiary amide trimers.

Table 4: Comparison of the transition temperatures and phase sequences of tertiary amide trimers and previously reported secondary trimers. N_{TB} – twist bend nematic, SmA_{bi} – smectic A with bilayer packing, SmA_C – smectic A with intercalated packing, SmC_A – smectic C with anticlinic intercalated structure, SmX – unknown smectic phase. * Temperatures taken from reference 19.

								
Core	n	N-X	SmX	SmC _A	SmA _C	SmA _{bi}	N _{TB}	N
	6	H*		• 168				• 298
		CH ₃				• 132		• 182
		Bn				• 147		• 111
	8	H*		• 152	• 186			• 283
		CH ₃				• 148		• 178
		Bn				• 143		• 148
	10	H*					• 145	• 267
		CH ₃				• 148		• 178
		Bn				• 144*		• 147*
	6	H*	• 199					• 298
		CH ₃						• 201
	6	H*						• 254
		CH ₃				• 130		• 175
	6	H*		• 199				• 296
		CH ₃				• 123		• 180

Conclusions

In summary, we report the synthesis and phase behaviour of a series of liquid crystal trimers containing tertiary benzanilides as the central mesogenic unit. These trimers form enantiotropic nematic and smectic A phases, which have been identified using POM, X-ray



diffraction, AFM and optical birefringence measurements. The unique structure of the *E*-amide conformation adopted by tertiary benzanilides gives these trimers an unusual, highly bent conformation, which we propose packs into a bilayer structure in the SmA phase. This structure greatly decreases the strength of the relationship between spacer length and phase transition temperatures, and for trimers with larger (decyl or benzyl) substituents on the amide nitrogen, an unusual decrease in the layer spacing is seen on cooling the smectic A phase. In addition, the phase sequences and transition temperatures of these trimers are much less sensitive to structural modifications than that of analogous trimers containing secondary benzanilides. These results demonstrate the use of tertiary benzanilides as components of liquid crystalline molecules forming nematic and smectic phases and opens new design possibilities for the development of novel mesogenic materials.

References

- 1 M. Hird, Banana-shaped and other bent-core liquid crystals, *Liq. Cryst. Today*, 2005, **14**, 9–21.
- 2 M. Cestari, S. Diez-Berart, D. A. Dunmur, A. Ferrarini, M. R. de la Fuente, D. J. B. Jackson, D. O. Lopez, G. R. Luckhurst, M. A. Perez-Jubindo, R. M. Richardson, J. Salud, B. A. Timimi and H. Zimmermann, Phase behavior and properties of the liquid-crystal dimer 1'',7''-bis(4-cyanobiphenyl-4'-yl) heptane: A twist-bend nematic liquid crystal, *Phys. Rev. E*, 2011, **84**, 031704.
- 3 V. Borshch, Y.-K. Kim, J. Xiang, M. Gao, A. Jáklí, V. P. Panov, J. K. Vij, C. T. Imrie, M. G. Tamba, G. H. Mehl and O. D. Lavrentovich, Nematic twist-bend phase with nanoscale modulation of molecular orientation, *Nat. Commun.*, 2013, **4**, 2365.
- 4 J. P. Abberley, R. Killah, R. Walker, J. M. D. Storey, C. T. Imrie, M. Salamończyk, C. Zhu, E. Gorecka and D. Pociecha, Helical smectic phases formed by achiral molecules, *Nat. Commun.*, 2018, **9**, 228.
- 5 T. Kato, N. Mizoshita and K. Kishimoto, Functional Liquid-Crystalline Assemblies: Self-Organized Soft Materials, *Angew. Chem. Int. Ed.*, 2006, **45**, 38–68.
- 6 J. W. Goodby, E. J. Davis, R. J. Mandle and S. J. Cowling, Nano-Segregation and Directed Self-Assembly in the Formation of Functional Liquid Crystals, *Isr. J. Chem.*, 2012, **52**, 863–880.
- 7 H. F. Gleeson, S. Kaur, V. Görtz, A. Belaissaoui, S. Cowling and J. W. Goodby, The Nematic Phases of Bent-Core Liquid Crystals, *ChemPhysChem*, 2014, **15**, 1251–1260.
- 8 P. A. Henderson and C. T. Imrie, Methylene-linked liquid crystal dimers and the twist-bend nematic phase, *Liq. Cryst.*, 2011, **38**, 1407–1414.
- 9 M. C. Varia, S. Kumar and A. K. Prajapati, H-shaped azoester-oxymethylene containing twin liquid crystalline compounds, *Liq. Cryst.*, 2012, **39**, 365–371.
- 10 R. Walker, D. Pociecha, A. Martinez-Felipe, J. M. Storey, E. Gorecka and C. T. Imrie, Twist-Bend Nematogenic Supramolecular Dimers and Trimers Formed by Hydrogen Bonding, *Crystals*, 2020, **10**, 175.
- 11 Y. Wang, G. Singh, D. M. Agra-Kooijman, M. Gao, H. Krishna Bisoyi, C. Xue, M. R. Fisch, S. Kumar and Q. Li, Room temperature helical twist-bend nematic liquid crystal, *CrystEngComm*, 2015, **17**, 2778–2782.
- 12 A. Yamaguchi, I. Nishiyama, J. Yamamoto, H. Yokoyama and A. Yoshizawa, Unusual smectic phases organized by novel λ -shaped mesogenic molecules, *J. Mater. Chem.*, 2005, **15**, 280–288.
- 13 J. Hobbs, M. Reynolds, M. Krishnappa Srinatha, G. Shanker, J. Mattsson and M. Nagaraj, The relaxation dynamics and dielectric properties of cyanobiphenyl-based nematic tripod liquid crystals, *J. Mol. Liq.*, 2023, **391**, 123069.
- 14 P. Henderson, A. Cook and C. Imrie, Oligomeric liquid crystals: From monomers to trimers Oligomeric liquid crystals: From monomers to trimers, *Liq. Cryst.*, 2004, **31**, 1427–1434.
- 15 T. Kajitani, S. Kohmoto, M. Yamamoto and K. Kishikawa, Generation of stable calamitic liquid-crystal phases with lateral intermolecular hydrogen bonding, *Chem. Mater.*, 2004, **16**, 2329–2331.



- 16 S. Kohmoto, M. Yamamoto, K. Kishikawa and T. Kajitani, Calamitic Liquid Crystalline Molecules with Lateral Intermolecular Hydrogen Bonding, *Mol. Cryst. Liq. Cryst.*, 2005, **439**, 173/[2039]-177/[2043].
- 17 G. Mohiuddin, S. Ghosh, N. Begum, S. Debnath, S. Turlapati, D. S. S. Rao and R. V. S. Nandiraju, Amide linkage in novel three-ring bent-core molecular assemblies: polar mesophases and importance of H-bonding, *Liq. Cryst.*, 2018, **45**, 1549–1566.
- 18 G. J. Strachan, W. T. A. Harrison, J. M. D. Storey and C. T. Imrie, Understanding the remarkable difference in liquid crystal behaviour between secondary and tertiary amides: the synthesis and characterisation of new benzanilide-based liquid crystal dimers, *Phys. Chem. Chem. Phys.*, 2021, **23**, 12600–12611.
- 19 G. J. Strachan, M. M. Majewska, D. Pocięcha, E. Gorecka, J. M. D. Storey and C. T. Imrie, Liquid crystal trimers containing secondary amide groups, *Liq. Cryst.*, 2024, 10.1080/02678292.2024.2382301.
- 20 M. J. Gim, D. A. Beller and D. K. Yoon, Morphogenesis of liquid crystal topological defects during the nematic-smectic A phase transition, *Nat. Commun.*, 2017, **8**, 1–9.
- 21 V. M. Pergamenschchik, I. Lelidis and V. A. Uzunova, Stripe domains in a nearly homeotropic nematic liquid crystal: A bend escaped state at a nematic–smectic- A transition, *Phys. Rev. E*, 2008, **77**, 041703.
- 22 I. Lelidis and G. Barbero, Novel surface-induced modulated texture in thick nematic samples, *Europhys. Lett. EPL*, 2003, **61**, 646–652.
- 23 L. Guo, K. Gomola, E. Gorecka, D. Pocięcha, S. Dhara, F. Araoka, K. Ishikawa and H. Takezoe, Transition between two orthogonal polar phases in symmetric bent-core liquid crystals, *Soft Matter*, 2011, **7**, 2895–2899.
- 24 K. Gomola, L. Guo, S. Dhara, Y. Shimbo, E. Gorecka, D. Pocięcha, J. Mieczkowski and H. Takezoe, Syntheses and characterization of novel asymmetric bent-core mesogens exhibiting polar smectic phases, *J. Mater. Chem.*, 2009, **19**, 4240–4247.
- 25 E. Cruickshank, G. J. Strachan, M. M. Majewska, D. Pocięcha, E. Gorecka, J. M. D. Storey and C. T. Imrie, The effects of alkylthio chains on the properties of symmetric liquid crystal dimers, *New J. Chem.*, 2023, **47**, 7356–7368.
- 26 Y. Lansac, M. A. Glaser and N. A. Clark, Microscopic structure and dynamics of a partial bilayer smectic liquid crystal, *Phys. Rev. E*, 2001, **64**, 051703.
- 27 S. Urban, J. Przedmojski and J. Czub, X-ray studies of the layer thickness in smectic phases, *Liq. Cryst.*, 2005, **32**, 619–624.
- 28 N. Podoliak, P. Salamon, L. Lejček, P. Kužel and V. Novotná, Undulations of Smectic A Layers in Achiral Liquid Crystals Manifested as Stripe Textures, *Phys. Rev. Lett.*, 2023, **131**, 228101.

Acknowledgements

MMM wishes to acknowledge NCBiR grant proposal number: EIG CONCERT-JAPAN/9/89/FerroFluid/2023.

Conflict of Interest

There are no conflicts of interest to declare.



The data supporting this article have been included as part of the Supplementary Information.

[View Article Online](#)
DOI: 10.1039/D5TC01532D



Supplementary Information

Liquid crystal trimers containing tertiary benzanilide groups.

Grant J. Strachan,^{a†} Magdalena Majewska,^b Ewan Cruickshank,^{a‡} Damian Pocięcha,^b Ewa Gorecka,^b John M.D. Storey,^a Corrie T. Imrie.^{a*}

*Author for correspondence: gj.strachan@outlook.com

^a Department of Chemistry, School of Natural and Computing Sciences, University of Aberdeen, Meston Building, Aberdeen, AB24 3UE, UK

^b Faculty of Chemistry, University of Warsaw, ul. Pasteura 1, 02-093 Warsaw, Poland

[†]Current address: Faculty of Chemistry, University of Warsaw, ul. Pasteura 1, 02-093 Warsaw, Poland

[‡]Current address: School of Pharmacy, Applied Sciences and Public Health, Robert Gordon University, Aberdeen, AB10 7GJ, UK

*Deceased 14th January 2025

Materials and methods

Unless otherwise stated, all materials were obtained from commercial sources and used without further purification. Where dry solvents were used, these were dried over 3 or 4 Å molecular sieves for at least 48 hours before use. Glassware used in anhydrous reactions was pre-dried in an oven set at 110 °C for at least 12 hours. Reactions were monitored using thin layer chromatography (TLC) using aluminium-backed plates with a coating of Merck Kieselgel 60 F254 silica and an appropriate solvent system. Spots were visualised using UV light (254 nm). Solvents were evaporated at approximately 20 mm Hg using a water aspirator pump connected to a rotary evaporator. Flash column chromatography was carried out using silica grade 60 Å 40-63 micron.

Instrumentation

Melting points and phase transition temperatures were measured by differential scanning calorimetry with a heating rate of 10 °C min⁻¹ unless otherwise specified. FT-IR spectra were obtained using a Perkin Elmer spectrum 2 FTIR with an ATR diamond cell. ¹H and ¹³C NMR spectra were recorded on a 300 MHz Bruker Ultrashield NMR spectrometer (300 MHz for ¹H NMR and 75 MHz for ¹³C NMR) or a 400 MHz Bruker Ascend NMR spectrometer (400 MHz for ¹H NMR and 100 MHz for ¹³C NMR) using either CDCl₃ or DMSO-*d*₆ as solvent and using residual non-deuterated trace solvents as reference. Chemical shifts (δ) are given in ppm relative to TMS (δ = 0.00 ppm). Coupling constants (J) are given in Hz and are vicinal (³J). Ar refers to an aromatic ring. Q-TOF mass spectrometry was performed at the University of Aberdeen on a Waters XEVO G2 Q-ToF, S/N YCA247K. Calibration: Sodium formate. Lock mass: leucine enkephalin, C₂₈H₃₇N₅O₇ [M+H]⁺: 556.2771

The phase behaviour of the materials was studied using differential scanning calorimetry (DSC) with a Mettler Toledo DSC3 differential scanning calorimeter equipped with a TSO 801RO sample robot and calibrated with indium and zinc standards. The heating and cooling rates were 10 K min⁻¹ and the transition temperatures and their associated enthalpy changes were extracted from heating traces unless otherwise noted.

Optical textures were used to identify the liquid crystal phases, and these were observed using an Olympus BH2 polarising optical microscope equipped with a Linkam TMS 92 heating stage. Optical birefringence was measured with a setup based on a photoelastic modulator (PEM-90, Hinds) working at a modulation frequency $f = 50$ kHz; a halogen lamp (Hamamatsu LC8) equipped with narrow bandpass filters was used as a light source. The signal from a photodiode (FLC Electronics PIN-20) was deconvoluted with a lock-in amplifier (EG&G 7265) into 1 f and 2 f components to yield a retardation induced by the sample. Knowing the sample thickness, the retardation was recalculated into optical birefringence. Samples were prepared in 3-micron-thick cells with planar anchoring. The alignment quality was checked prior to measurement by inspection under the polarised optical microscope.

AFM measurements were performed using a Bruker Dimension Icon Microscope working in tapping or scan assist mode and cantilevers with elastic constant of 0.4 N/m were applied.

X-ray diffraction measurements were carried out using a Bruker D8 GADDS system with CuK α radiation, Goebel mirror monochromator, point beam collimator, and VANTEC2000 area detector. SAXS measurements were performed on a Bruker Nanostar system using CuK α radiation and patterns were collected with an area detector VANTEC2000.

Synthetic procedures

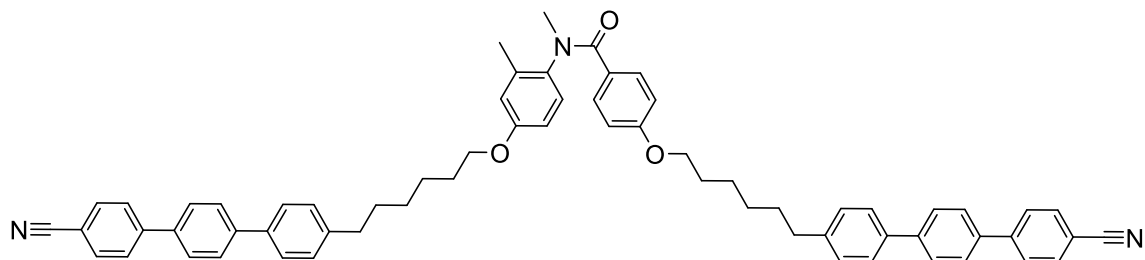
The tertiary amides reported here were prepared by alkylation of the corresponding secondary benzanilide, the synthesis of which is reported elsewhere.¹

General method: N-alkylation

The amide was dried by azeotropic distillation with toluene (3 x 2ml). Sodium hydride (60% dispersion, 2.5 eq) was washed with petroleum ether (3 x 1 ml). The amide was dissolved in dry THF and added to the NaH under an argon atmosphere. When reaction was complete (fizzing stops) the reaction was left for a further 30 min and then the appropriate alkyl iodide or benzyl bromide (2.5 eq) was added and the reaction was followed by TLC. When the reaction was deemed complete the excess NaH was quenched with a few drops of propanol, and the THF was removed under vacuum (3 mmHg). The crude solid was dissolved in chloroform (30 ml) and washed with water (3 x 25 ml). The organic layer is dried and removed *in vacuo*. The crude solid was dissolved in the minimum amount of chloroform (2-

10 ml) and methanol added dropwise until a precipitate begins to form. This was collected by vacuum filtration.

4-[[6-(3⁴-cyano[1¹,2¹:2⁴,3¹-terphenyl]-1⁴-yl)hexyl]oxy]-*N*-(4-[[6-(3⁴-cyano[1¹,2¹:2⁴,3¹-terphenyl]-1⁴-yl)hexyl]oxy)-2-methylphenyl)-*N*-methylbenzamide 1



amide	0.415 g	0.4 mmol
NaH	0.045 g	1.1 mmol
CH ₃ I	0.08 mL	1.1 mmol
THF	15 mL	

12 h at RT

Yield 0.318 g (85%).

Cr 102 °C Sm 132 °C N 182 °C I

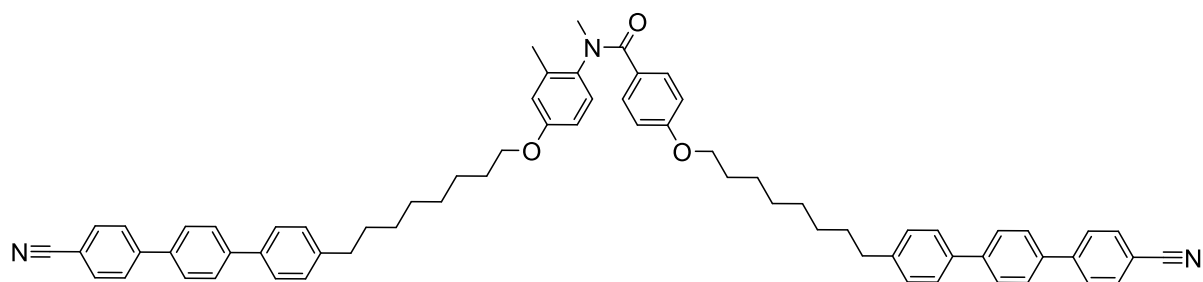
M/Z Calculated mass [M+H]: 932.4791 (C₆₅H₆₂N₃O₃) Found 932.4828 Difference 4.0 ppm.

ν_{\max} /cm⁻¹: 2926 (CH₂), 2854 (CH₂), 2226 (CN), 1635 (C=O), 1604 (Ar), 1004 (Ar), 812 (Ar).

¹H NMR (400 MHz, Chloroform-*d*) δ 7.76 (overlapping doublets, 8H, Ar-H), 7.72 (d, *J* = 8.4 Hz, 4H, Ar-H), 7.68 (d, *J* = 8.5 Hz, 4H, Ar-H), 7.57 (overlapping doublets, 4H, Ar-H), 7.29 (overlapping doublets, 6H, Ar-H), 6.96 (6.97 (d, *J* = 8.4 Hz, 1H, Ar-H), 6.66 (overlapping doublets and singlet, 4H, Ar-H), 3.90 (overlapping triplets, 4H, O-CH₂), 3.35 (s, 3H, N-CH₃), 2.69 (overlapping triplets, 4H, Ar-CH₂), 2.16 (s, 3H, Ar-CH₃), 1.81 – 1.64 (m, 8H, CH₂-CH₂), 1.59 – 1.41 (m, 8H, CH₂-CH₂-CH₂).

¹³C NMR (101 MHz, Chloroform-*d*) δ 170.45, 159.99, 157.98, 145.18, 145.16, 142.40 (2C), 141.44, 141.43, 137.65, 137.62, 137.55, 137.53, 136.89, 135.96, 132.64 (4C), 130.40 (2C), 129.29, 128.98 (4C), 127.94, 127.58 (4C), 127.56 (4C), 127.52 (4C), 126.92 (4C), 118.97 (2C), 116.66, 113.29 (2C), 112.76, 110.84, 110.82, 67.97, 67.78, 38.02, 35.50, 35.49, 31.34, 31.31, 29.18, 29.08, 29.02, 28.99, 25.92, 25.87, 18.03.

4-[[8-(3⁴-cyano[1¹,2¹:2⁴,3¹-terphenyl]-1⁴-yl)octyl]oxy]-*N*-(4-[[8-(3⁴-cyano[1¹,2¹:2⁴,3¹-terphenyl]-1⁴-yl)octyl]oxy)-2-methylphenyl)-*N*-methylbenzamide 2



Amide	0.360	0.37 mmol
NaH	0.037 g	0.93 mmol
CH ₃ I	0.05 mL	0.89 mmol
THF	20 mL	

17 h at RT

Yield 0.079 g (22%)

Cr 106 °C Sm 148 °C N 178 °C I

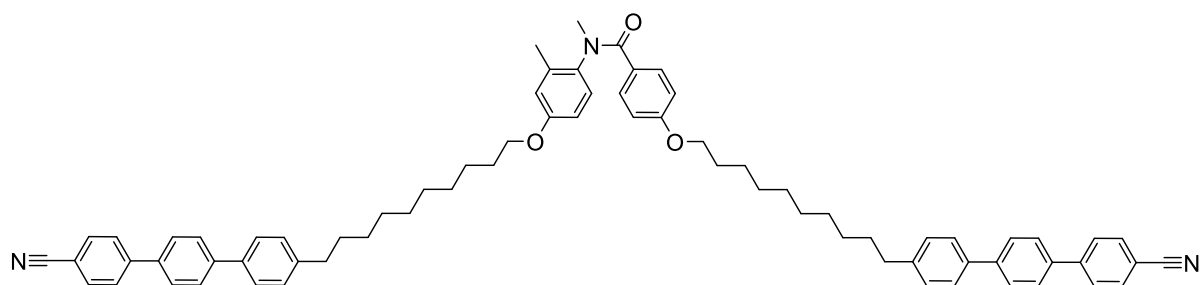
M/Z Calculated mass [M+Na]: 1010.5237 (C₆₉H₆₉N₃O₃Na) Found 1010.5252. Difference 1.5 ppm.

$\nu_{\max}/\text{cm}^{-1}$: 2926 (CH₂), 2854 (CH₂), 2226 (CN), 1636 (C=O), 1604 (Ar), 1004 (Ar), 812 (Ar).

¹H NMR (400 MHz, Chloroform-*d*) δ 7.76 (overlapping doublets, 8H, Ar-H), 7.72 (d, *J* = 9.0 Hz, 4H, Ar-H), 7.68 (d, *J* = 9.0 Hz, 4H, Ar-H), 7.58 (overlapping doublets, 4H, Ar-H), 7.31 (d, *J* = 2.7 Hz, 4H, Ar-H), 7.26 (d, *J* = 8.4 Hz, 2H, Ar-H), 6.96 (d, *J* = 8.4 Hz, 1H, Ar-H), 6.64 (overlapping doublets and singlet, 4H, Ar-H), 3.89 (overlapping triplets, 4H, O-CH₂), 3.34 (s, 3H, N-CH₃), 2.68 (overlapping triplets, 4H, Ar-CH₂), 2.15 (s, 3H, Ar-CH₃), 1.79 – 1.74 (m, 4H, O-CH₂-CH₂), 1.77 – 1.64 (m, 4H, Ar-CH₂-CH₂), 1.45 – 1.34 (m, 16H, CH₂-CH₂-CH₂).

¹³C NMR (101 MHz, CDCl₃) δ 170.42, 160.02, 158.00, 145.20, 145.18, 142.60 (2C), 141.50, 141.48, 137.65, 137.62, 137.52, 137.49, 136.91, 135.97, 132.64 (4C), 130.41 (2C), 129.29, 128.98 (4C), 127.95, 127.60 (4C), 127.56 (4C), 127.52 (4C), 126.91 (4C), 118.97 (2C), 116.66, 113.29 (2C), 112.75, 110.87, 110.85, 68.06, 67.86, 38.02, 35.63, 35.61, 31.46, 31.43, 29.44, 29.40, 29.33, 29.29 (2C), 29.25 (2C), 29.15, 26.05, 25.99, 18.04.

4-{[10-(3⁴-cyano[1¹,2¹:2⁴,3¹-terphenyl]-1⁴-yl)decyl]oxy}-*N*-(4-{[10-(3⁴-cyano[1¹,2¹:2⁴,3¹-terphenyl]-1⁴-yl)decyl]oxy}-2-methylphenyl)-*N*-methylbenzamide 3



Amide	0.400	0.4 mmol
NaH	0.050 g	1.3 mmol
CH ₃ I	0.06 mL	1.0 mmol
THF	50 mL	

15 h at RT

Recrystallised 25 ml EtOH

Yield 0.236 g (57%)

Cr 100 °C Sm 148 °C N 178 °C I

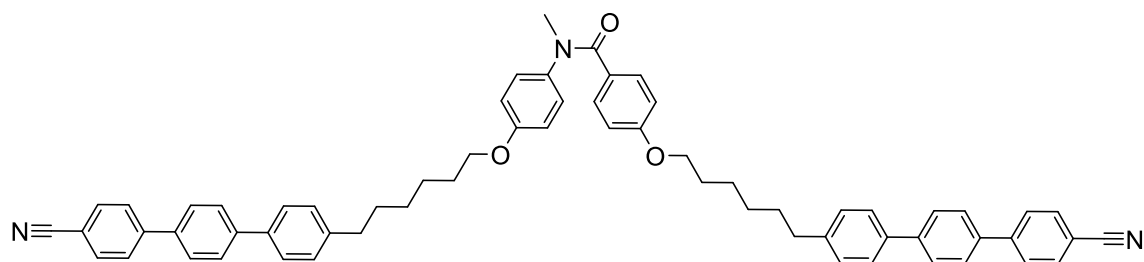
M/Z Calculated mass [M+H]: 1044.6043 (C₇₃H₇₈N₃O₃) Found 1044.6084. Difference 3.9 ppm.

ν_{max}/cm^{-1} : 2926 (CH₂), 2854 (CH₂), 2225 (CN), 1634(C=O), 1604 (Ar), 1004 (Ar), 812 (Ar).

¹H NMR (400 MHz, Chloroform-*d*) δ 7.66 (overlapping doublets, 8H, Ar-H), 7.63 (d, *J* = 8.3 Hz, 4H, Ar-H), 7.59 (d, *J* = 8.3 Hz, 4H, Ar-H), 7.48 (d, *J* = 7.8 Hz, 4H, Ar-H), 7.21 (overlapping doublets, 6H, Ar-H), 6.87 (d, *J* = 8.9 Hz, 1H, Ar-H), 6.55 (overlapping doublet and singlet, 4H, Ar-H), 3.79 (overlapping triplets, 4H, O-CH₂), 3.25 (s, 3H, N-CH₃), 2.58 (t, *J* = 8.0 Hz, 4H, Ar-CH₂), 2.05 (s, 3H, Ar-CH₃), 1.81 – 1.52 (m, 12H, CH₂-CH₂), 1.42 – 1.16 (m, 20H, CH₂-CH₂-CH₂).

¹³C NMR (101 MHz, Chloroform-*d*) δ 170.54 (HMBC), 160.02, 158.01, 145.21, 145.19, 142.68 (2C), 141.52 (2C), 137.64, 137.62, 137.49, 137.47, 136.90, 135.96, 132.64 (4C), 130.41 (4C), 129.29, 128.98 (4C), 127.60 (4C), 127.56 (4C), 127.52 (4C), 126.94, 126.90 (4C), 118.97 (2C), 116.66, 113.29 (2C), 112.75, 110.85, 68.09, 67.89, 38.02, 35.64, 31.50, 31.48, 29.56, 29.53, 29.53 (2C), 29.49, 29.49, 29.39, 29.38, 29.36, 29.34, 29.26, 29.16, 26.04, 26.00, 18.04.

4-{[6-(3⁴-cyano[1¹,2¹:2⁴,3¹-terphenyl]-1⁴-yl)hexyl]oxy}-*N*-(4-{[6-(3⁴-cyano[1¹,2¹:2⁴,3¹-terphenyl]-1⁴-yl)hexyl]oxy}phenyl)-*N*-methylbenzamide 4



Amide	0.250	0.29 mmol
NaH	0.029 g	0.75 mmol
CH ₃ I	0.06 mL	1.0 mmol
THF	50 mL	

62 h at RT

Yield 0.075 g (28 %).

M/Z Calculated mass [M+H]: 918.4635 (C₆₄H₆₀N₃O₃) Found 918.4636. Difference 0.1 ppm.

M/Z Calculated mass [M+Na]: 940.4454 (C₆₄H₅₉N₃O₃Na) Found 940.4420. Difference -3.6 ppm.

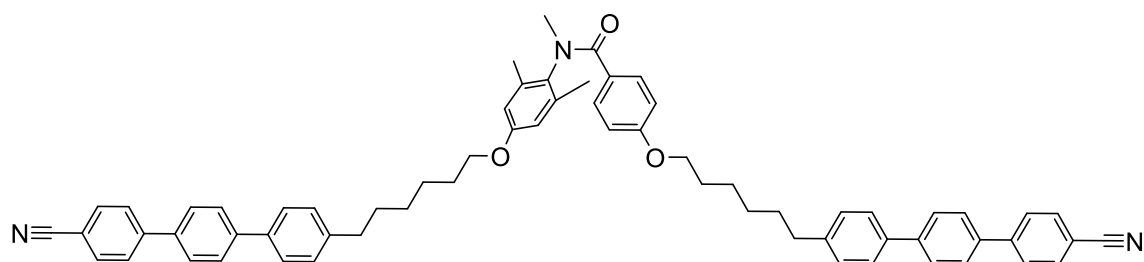
Cr 92 °C N 201 °C I

ν_{max}/cm^{-1} : 2926 (CH₂), 2854 (CH₂), 2226 (CN), 1636 (C=O), 1604 (Ar), 1004 (Ar), 813 (Ar).

¹H NMR (400 MHz, Chloroform-*d*) δ 7.76 (overlapping doublets, 8H, Ar-H), 7.72 (d, *J* = 8.5 Hz, 4H, Ar-H), 7.68 (d, *J* = 8.5 Hz, 4H, Ar-H), 7.57 (overlapping doublets, 4H, Ar-H), 7.29 (overlapping doublets, 6H, Ar-H), 6.97 (d, *J* = 8.8 Hz, 2H, Ar-H), 6.76 (d, *J* = 8.5 Hz, 2H, Ar-H), 6.68 (d, *J* = 8.8 Hz, 2H, Ar-H), 3.91 (t, *J* = 6.4 Hz, 4H, O-CH₂), 3.345 (s, 3H, N-CH₃), 45 (s, 3H), 2.69 (overlapping triplets, 4H, Ar-CH₂), 1.85 – 1.62 (m, 8H, CH₂-CH₂), 1.58 – 1.35 (m, 8H, CH₂-CH₂-CH₂).

¹³C NMR (101 MHz, Chloroform-*d*) δ 170.34, 160.02, 157.30, 145.21, 145.19, 142.40, 141.46, 141.44, 137.68, 137.65, 137.57, 137.55, 132.71, 132.64 (4C), 132.31, 130.83 (2C), 128.98 (4C), 127.94, 127.87, 127.80, 127.59 (4C), 127.57 (4C), 127.53 (4C), 126.93 (4C), 118.96 (2C), 114.91, 114.21, 113.44 (2C), 110.86 (2C), 68.10, 67.82, 38.91, 35.50, 35.43, 31.32, 31.27, 29.15, 29.09, 29.02, 28.99, 25.92, 25.88.

4-{[6-(3⁴-cyano[1¹,2¹:2⁴,3¹-terphenyl]-1⁴-yl)hexyl]oxy}-N-(4-{[6-(3⁴-cyano[1¹,2¹:2⁴,3¹-terphenyl]-1⁴-yl)hexyl]oxy}-2,6-dimethylphenyl)-N-methylbenzamide 5



Amide	0.470	0.5 mmol
NaH	0.058 g	1.5 mmol
CH ₃ I	0.08 mL	1.3 mmol
THF	50 mL	

14 h at RT

Yield 0.144 g (30 %).

Cr 98 °C Sm 130 °C N 175 °C I

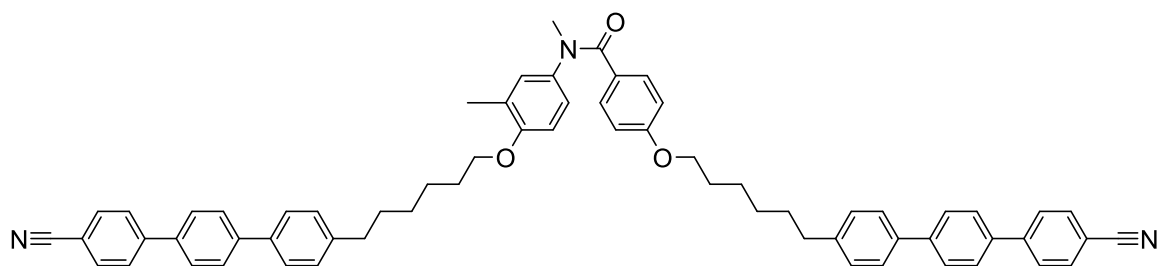
M/Z Calculated mass [M+Na]: 968.4767 (C₆₆H₆₃N₃O₃Na) Found 968.4747. Difference -2.1 ppm.

ν_{max}/cm^{-1} : 2922 (CH₂), 2851 (CH₂), 2227 (CN), 1650 (C=O), 1604 (Ar), 1003 (Ar), 810 (Ar).

¹H NMR (400 MHz, Chloroform-*d*) δ 7.76 (overlapping doublets, 8H, Ar-H), 7.72 (d, *J* = 8.4 Hz, 4H, Ar-H), 7.68 (d, *J* = 8.4 Hz, 4H, Ar-H), 7.57 (overlapping doublets, 4H, Ar-H), 7.28 (overlapping doublets, 6H, Ar-H), 6.65 (d, *J* = 8.6 Hz, 2H, Ar-H), 6.54 (s, 2H, Ar-H), 3.89 (overlapping triplets, 4H, O-CH₂), 3.28 (s, 3H, N-CH₃), 2.69 (overlapping triplets, 4H, Ar-CH₂), 2.17 (s, 6H, Ar-CH₃), 1.80 – 1.65 (m, 8H, CH₂-CH₂), 1.52 – 1.43 (m, 8H, CH₂-CH₂-CH₂).

¹³C NMR (101 MHz, Chloroform-*d*) δ 170.18, 160.18, 157.85, 145.19, 145.17, 142.40 (2C), 141.47, 141.44, 137.68, 137.65, 137.58, 137.56, 136.48 (2C), 135.78, 132.64 (4C), 129.95 (2C), 128.98 (4C), 127.84, 127.60 (4C), 127.56 (4C), 127.52 (4C), 126.93 (4C), 118.97 (2C), 114.32 (2C), 113.24 (2C), 110.88, 110.86, 67.84, 67.78, 36.74, 35.52, 35.50, 31.36, 31.32, 29.23, 29.09, 29.05, 29.01, 25.94, 25.89, 18.36 (2C).

4-[[6-(3⁴-cyano[1¹,2¹:2⁴,3¹-terphenyl]-1⁴-yl)hexyl]oxy}-*N*-(4-[[6-(3⁴-cyano[1¹,2¹:2⁴,3¹-terphenyl]-1⁴-yl)hexyl]oxy)-3-methylphenyl)-*N*-methylbenzamide 6



Amide	0.461	0.5 mmol
NaH	0.054 g	1.4 mmol
CH ₃ I	0.08 mL	1.3 mmol
THF	20 mL	

13 h at RT

Yield 0.045g (10 %).

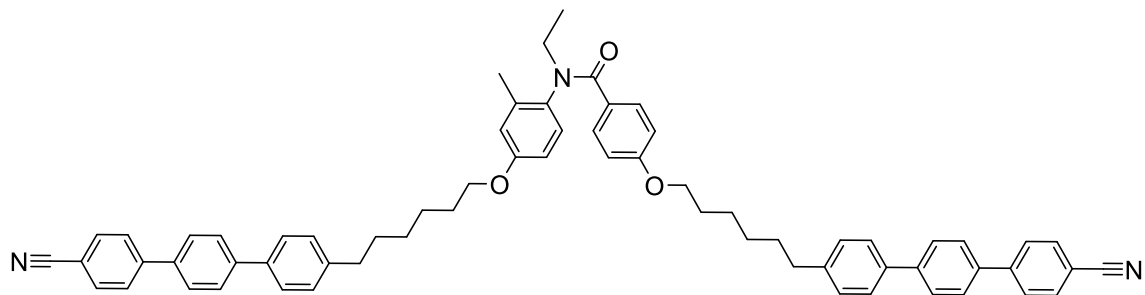
Cr 97 °C Sm 123 °C N 180 °C I

M/Z Calculated mass [M+H]: 932.4791 (C₆₅H₆₂N₃O₃) Found 932.4767. Difference -2.6 ppm. $\nu_{\max}/\text{cm}^{-1}$: 2924(CH₂), 2853 (CH₂), 2227 (CN), 1639 (C=O), 1604 (Ar), 1004 (Ar), 811 (Ar).

¹H NMR (400 MHz, Chloroform-*d*) δ 7.76 (overlapping doublets, 8H, Ar-H), 7.72 (d, *J* = 8.7 Hz, 4H, Ar-H), 7.68 (d, *J* = 8.7 Hz, 4H, Ar-H), 7.57 (overlapping doublets, 4H, Ar-H), 7.30 (d, *J* = 5.0 Hz, 4H, Ar-H), (7.29 HSQC, 2H, Ar-H), 6.90 (d, *J* = 2.6 Hz, 1H, Ar-H), 6.77 (dd, *J* = 8.6, 2.7 Hz, 1H, Ar-H), 6.67 (d, *J* = 8.8 Hz, 2H, Ar-H), 6.63 (d, *J* = 8.6 Hz, 1H, Ar-H), 3.91 (t, *J* = 6.4 Hz, 4H, O-CH₂), 3.44 (s, 3H, N-CH₃), 2.69 (q, *J* = 7.2 Hz, 4H, Ar-CH₂), 2.16 (s, 3H, Ar-CH₃), 1.87 – 1.64 (m, 8H, CH₂-CH₂), 1.62 – 1.39 (m, 8H, CH₂-CH₂-CH₂).

¹³C NMR (101 MHz, Chloroform-*d*) δ 170.24, 159.93, 155.47, 145.19, 145.17, 143.94, 142.40 (2C), 141.47, 141.44, 137.68, 137.65, 137.58, 137.56, 132.65 (4C), 130.81 (2C), 128.98 (4C), 128.81, 128.08, 127.73, 127.59 (4C), 127.57 (4C), 127.52 (4C), 126.93 (4C), 125.26, 118.97 (2C), 113.39 (2C), 110.94, 110.88, 110.86, 68.04, 67.82, 39.00, 35.53, 35.50, 31.38, 31.32, 29.24, 29.10, 29.03, 29.00, 26.03, 25.88, 16.27.

4-{[6-(3⁴-cyano[1¹,2¹:2⁴,3¹-terphenyl]-1⁴-yl)hexyl]oxy}-*N*-(4-{[6-(3⁴-cyano[1¹,2¹:2⁴,3¹-terphenyl]-1⁴-yl)hexyl]oxy}-2-methylphenyl)-*N*-ethylbenzamide 7



Amide	0.099g	0.11 mmol
NaH	0.022 g	0.55 mmol
C ₂ H ₅ I	0.02 mL	0.25 mmol
THF	15 mL	

88 h at RT, then 52 h at 35 °C

Column chromatography 7 % EtOAc / toluene, R_f 0.18

Yield 0.02 g (20 %).

Cr 100 °C Sm 123 °C N 154 °C I

M/Z Calculated mass [M+H]: 946.4948 (C₆₆H₆₄N₃O₃) Found 946.4916. Difference -3.4 ppm.

M/Z Calculated mass [M+Na]: 968.4767 (C₆₆H₆₃N₃O₃Na) Found 968.4720. Difference -4.9 ppm.

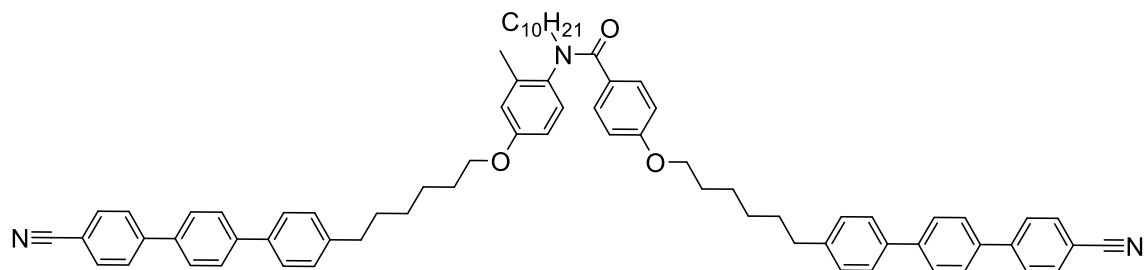
 $\nu_{\max}/\text{cm}^{-1}$: 2925 (CH₂), 2854 (CH₂), 2226 (CN), 1635 (C=O), 1604 (Ar), 1004 (Ar), 812 (Ar).

^1H NMR (400 MHz, Chloroform-*d*) δ 7.76 (overlapping doublets, 8H, Ar-H), 7.72 (d, $J = 8.2$ Hz, 4H, Ar-H), 7.68 (d, $J = 8.2$ Hz, 4H, Ar-H), 7.58 (overlapping doublets, 4H, Ar-H), 7.27 (overlapping doublets, 6H, Ar-H), 6.97 (d, $J = 9.0$ Hz, 1H, Ar-H), 6.64 (overlapping doublets, $J = 9.7$ Hz, 4H, Ar-H), 4.12 – 4.03 (m, 1H, N-CH), 3.90 (overlapping triplets, 4H, O-CH₂), 3.66 – 3.56 (m, 1H, N-CH), 2.69 (overlapping triplets, 4H, Ar-CH₂), 2.12 (s, 3H, Ar-CH₃), 1.82 – 1.67 (m, 8H, CH₂-CH₂), 1.55 – 1.39 (m, 8H, CH₂-CH₂-CH₂), 1.21 (t, $J = 7.2$ Hz, 3H, CH₂-CH₃).

^{13}C NMR (101 MHz, Chloroform-*d*) δ 169.78, 159.85, 157.90, 145.19, 145.16, 142.41 (2C), 141.46, 141.44, 137.68, 137.64, 137.57, 137.55, 136.51, 134.99, 132.66 (4C), 130.38 (2C), 130.28, 128.99 (4C), 128.48, 127.60 (4C), 127.58 (4C), 127.53 (4C), 126.94 (4C), 119.00 (2C), 116.57, 113.23 (2C), 112.48, 110.87, 110.84, 67.94, 67.76, 44.96, 35.53, 35.51, 31.38, 31.35, 29.22, 29.10, 29.06, 29.02, 25.95, 25.89, 18.28, 12.50.

^{13}C NMR (101 MHz, Chloroform-*d*) δ 170.45, 159.99, 157.98, 145.18, 145.16, 142.40 (2C), 141.44, 141.43, 137.65, 137.62, 137.55, 137.53, 136.89, 135.96, 132.64 (4C), 130.40 (2C), 129.29, 128.98 (4C), 127.94, 127.58 (4C), 127.56 (4C), 127.52 (4C), 126.92 (4C), 118.97 (2C), 116.66, 113.29 (2C), 112.76, 110.84, 110.82, 67.97, 67.78, 38.02, 35.50, 35.49, 31.34, 31.31, 29.18, 29.08, 29.02, 28.99, 25.92, 25.87, 18.03.

4-{[6-(3⁴-cyano[1¹,2¹:2⁴,3¹-terphenyl]-1⁴-yl)hexyl]oxy}-*N*-(4-{[6-(3⁴-cyano[1¹,2¹:2⁴,3¹-terphenyl]-1⁴-yl)hexyl]oxy}-2-methylphenyl)-*N*-decylbenzamide 8



Amide	0.571 g	0.6 mmol
NaH	0.056 g	1.4 mmol
C ₁₀ H ₂₁ I	0.05 mL	0.23 mmol
THF	50 mL	

12 h at RT followed by 50 h at reflux

Recrystallise from EtOAc (25 ml), then dissolve in CHCl₃ (2 mL) and add MeOH until a precipitate forms.

Yield 0.023 g, (4 %)

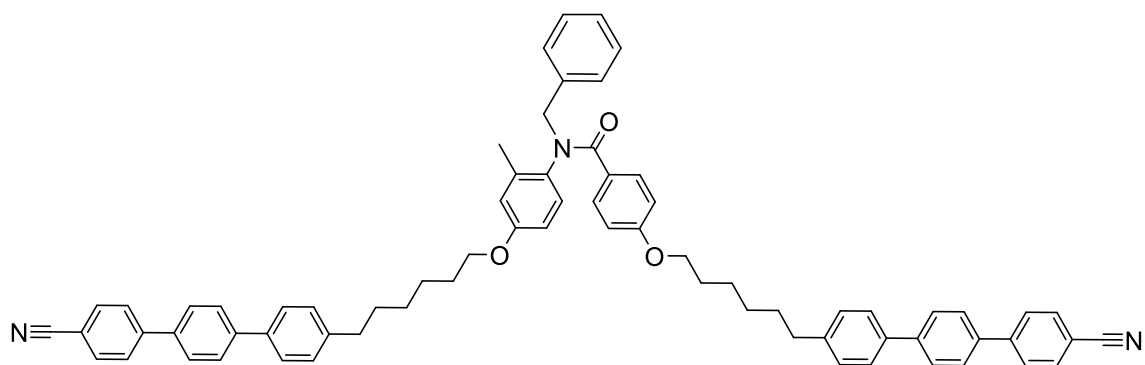
Cr 108 °C Sm 131 °C N 143 °C I

M/Z Calculated mass [M+Na]: 1080.6019 (C₇₄H₇₉N₃O₃Na) Found 1080.6003. Difference -1.5 ppm.

$\nu_{\max}/\text{cm}^{-1}$: 2928 (CH_2), 2855 (CH_2), 2227 (CN), 1637 (C=O), 1605 (Ar), 1004 (Ar), 812 (Ar).
 ^1H NMR (400 MHz, Chloroform-*d*) δ 7.76 (overlapping doublets, 8H, Ar-H), 7.71 (d, J = 8.4 Hz, 4H, Ar-H), 7.68 (d, J = 8.4 Hz, 4H, Ar-H), 7.57 (overlapping doublets, 4H, Ar-H), 7.30 (overlapping doublets, 4H, Ar-H), 7.23 (d, J = 8.5 Hz, 2H, Ar-H), 6.97 (d, J = 8.5 Hz, 1H, Ar-H), 6.63 (overlapping doublets and singlet, 4H, Ar-H), 4.06 – 4.01 (m, 2H, N-CH₂), 3.90 (overlapping triplets, 4H, O-CH₂), 3.54 – 3.40 (m, 1H, N-CH₂), 2.69 (overlapping triplets, 4H, Ar-CH₂), 2.10 (s, 3H, Ar-CH₃), 1.83 – 1.65 (m, 8H, CH₂-CH₂), 1.52 – 1.43 (m, 8H, CH₂-CH₂-CH₂), 1.33 – 1.19 (m, 16H CH₂-CH₂-CH₂), 0.90 (t, J = 6.8 Hz, 3H, CH₂-CH₃).

^{13}C NMR (101 MHz, Chloroform-*d*) not all peaks could be identified due to overlapping signals in aliphatic region δ 169.85, 159.81, 157.88, 145.19, 145.17, 142.50, 142.41 (2C), 141.51, 141.47, 141.45, 137.68, 137.64, 137.58, 137.55, 135.37, 132.64 (4C), 130.35 (2C), 130.20, 128.98 (4C), 128.58, 127.61, 127.60 (4C), 127.56 (4C), 127.52 (4C), 126.94 (4C), 118.97 (2C), 116.57, 113.22 (2C), 112.47, 110.88, 110.86, 67.96, 67.77, 50.11, 35.53, 35.50, 31.90, 31.36, 31.32, 29.73, 29.63, 29.56, 29.46, 29.30, 29.22, 29.09, 29.06, 29.00, 27.31, 27.19, 25.95, 25.88, 22.69, 18.27, 14.13.

4-{[6-(3⁴-cyano[1¹,2¹:2⁴,3¹-terphenyl]-1⁴-yl)hexyl]oxy}-*N*-(4-{[6-(3⁴-cyano[1¹,2¹:2⁴,3¹-terphenyl]-1⁴-yl)hexyl]oxy}-2-methylphenyl)-*N*-benzylbenzamide 9



Amide	0.189 g	0.2 mmol
NaH	0.024 g	0.6 mmol
Benzyl bromide	0.05 mL	0.42 mmol
THF	10 mL	

48 h at RT

Column chromatography (5 % EtOAc / toluene, R_f 0.18)

Yield 0.098 g (50 %).

Cr 111 °C Sm 133 °C N 147 °C I

M/Z Calculated mass $[\text{M}+\text{H}]$: 1008.5104 ($\text{C}_{71}\text{H}_{66}\text{N}_3\text{O}_3$) Found 1008.5074. Difference -3.0 ppm.

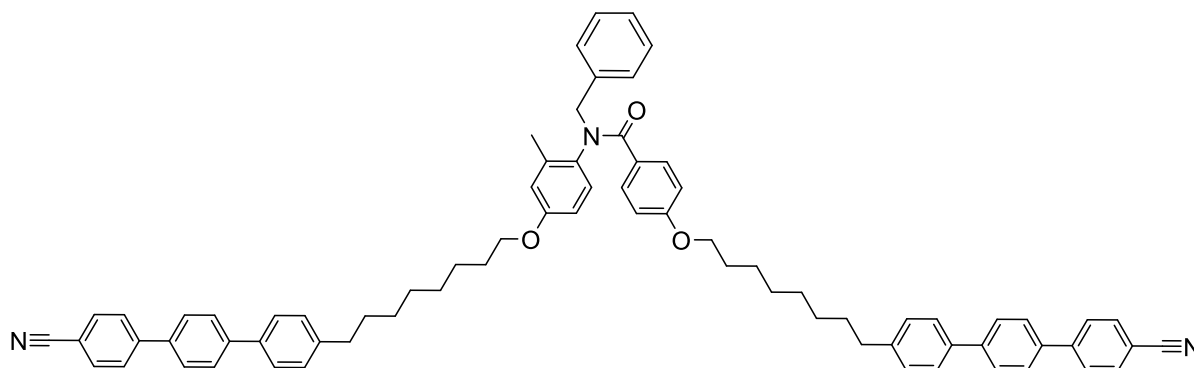
M/Z Calculated mass [M+Na]: 1030.4924 (C₇₁H₆₅N₃O₃Na) Found 1030.4950. Difference 2.5 ppm.

$\nu_{\max}/\text{cm}^{-1}$: 2926 (CH₂), 2855 (CH₂), 2226 (CN), 1633 (C=O), 1604 (Ar), 1004 (Ar), 811 (Ar).

¹H NMR (400 MHz, Chloroform-*d*) δ 7.76 (overlapping doublets, 8H, Ar-H), 7.72 (d, *J* = 8.2 Hz, 4H, Ar-H), 7.68 (d, *J* = 8.2 Hz, 4H, Ar-H), 7.57 (overlapping doublets, 4H, Ar-H), 7.29 (overlapping peaks, 11H, Ar-H), 6.82 (d, *J* = 8.5 Hz, 1H, Ar-H), 6.63 (d, *J* = 8.5 Hz, 2H, Ar-H), 6.57 (overlapping doublet and singlet, 2H, Ar-H) 5.29 (d, *J* = 14.0 Hz, 1H, N-CH), 4.66 (d, *J* = 13.9 Hz, 1H, N-CH), 3.89 (t, *J* = 5.7 Hz, 4H, O-CH₂), 2.69 (overlapping triplets, 4H, Ar-CH₂), 1.84 (s, 3H, Ar-CH₃), 1.81 – 1.65 (m, 8H, CH₂-CH₂), 1.51 – 1.43 (m, 8H, CH₂-).

¹³C NMR (101 MHz, Chloroform-*d*) δ 169.95, 159.99, 157.95, 145.19, 145.16, 142.40 (2C), 141.46, 141.44, 137.68, 137.64, 137.58, 137.55, 137.37, 136.77, 134.96, 132.65 (4C), 130.55 (2C), 130.16 (2C), 129.45 (2C), 128.98 (4C), 128.26, 128.18, 127.59 (4C), 127.57 (4C), 127.52 (4C), 127.36, 126.94 (2C), 126.93 (2C), 118.97 (2C), 116.44, 113.23 (2C), 112.43, 110.88, 110.86, 67.90, 67.78, 53.70, 35.53, 35.50, 31.35, 31.32, 29.22, 29.09, 29.07, 29.00, 25.94, 25.88, 18.02.

4-([8-(3⁴-cyano[1¹,2¹:2⁴,3¹-terphenyl]-1⁴-yl)octyl]oxy)-*N*-(4-([8-(3⁴-cyano[1¹,2¹:2⁴,3¹-terphenyl]-1⁴-yl)octyl]oxy)-2-methylphenyl)-*N*-benzylbenzamide 10



Amide	0.062	0.063 mmol
NaH	0.032 g	0.80 mmol
Benzyl bromide	0.04 mL	0.71 mmol
THF	10 mL	

48 h at RT

Yield 0.032 g (48 %)

Cr 117 °C Sm 143 °C N 148 °C I

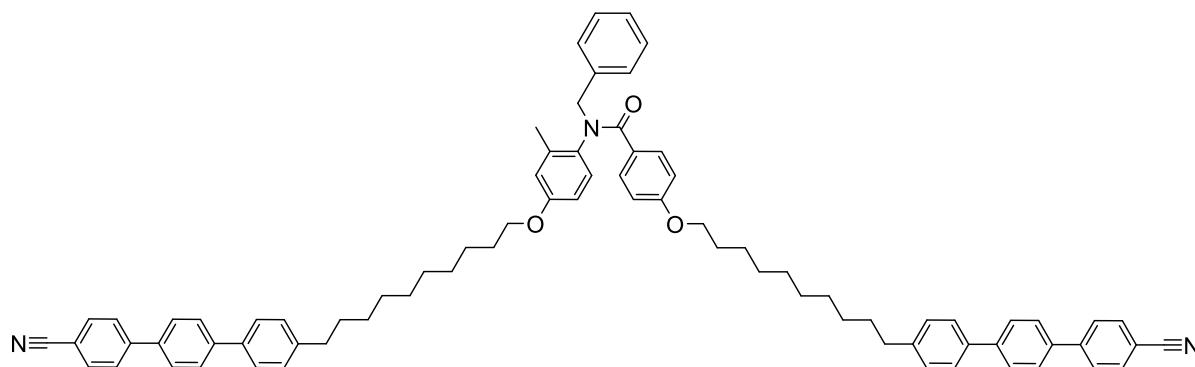
M/Z Calculated mass [M+Na]: 1086.5550 (C₇₅H₇₃N₃O₃Na) Found 1086.5601. Difference 4.7 ppm.

$\nu_{\max}/\text{cm}^{-1}$: 2924 (CH₂), 2853 (CH₂), 2226 (CN), 1639 (C=O), 1605 (Ar), 1004 (Ar), 813 (Ar).

^1H NMR (400 MHz, Chloroform-*d*) δ 7.76 (overlapping doublets, 8H, Ar-H), 7.72 (d, J = 8.4 Hz, 4H, Ar-H), 7.68 (d, J = 8.4 Hz, 4H, Ar-H), 7.57 (overlapping doublets, 4H, Ar-H), 7.29 (overlapping signals, 11H, Ar-H), 6.82 (d, J = 8.6 Hz, 1H, Ar-H), 6.63 (d, J = 8.4 Hz, 2H, Ar-H), 6.57 (overlapping doublet and singlet, 2H, Ar-H), 5.29 (d, J = 13.9 Hz, 1H, N-CH), 4.66 (d, J = 13.9 Hz, 1H, N-CH), 3.87 (overlapping triplets, 4H, O-CH₂), 2.68 (overlapping triplets, 4H, Ar-CH₂), 1.84 (s, 3H, Ar-CH₃), 1.80 – 1.64 (m, 8H, CH₂-CH₂), 1.42 – 1.34 (m, 16H, CH₂-CH₂-CH₂).

^{13}C NMR (101 MHz, CDCl₃) δ 170.02 (HMBC), 160.01, 157.96, 145.20, 145.18, 142.59 (2C), 141.50, 141.48, 137.65, 137.63, 137.52, 137.49, 137.38, 136.74, 134.94, 132.64 (4C), 130.54 (2C), 130.13 (2C), 129.44 (2C), 128.97 (4C), 128.25, 128.15, 127.59 (4C), 127.56 (4C), 127.52 (4C), 127.35, 126.91 (4C), 118.97 (2C), 116.44, 113.22 (2C), 112.43, 110.87, 110.85, 67.97, 67.86, 53.69, 35.63, 35.61, 31.46, 31.43, 29.43, 29.39, 29.34, 29.32, 29.29, 29.27, 29.24, 29.14, 26.06, 25.98, 18.01.

4-[[10-(3⁴-cyano[1¹,2¹:2⁴,3¹-terphenyl]-1⁴-yl)decyl]oxy]-*N*-(4-[[10-(3⁴-cyano[1¹,2¹:2⁴,3¹-terphenyl]-1⁴-yl)decyl]oxy)-2-methylphenyl)-*N*-benzylbenzamide 11



Amide	0.515	0.50 mmol
NaH	0.050 g	1.3 mmol
Benzyl bromide	0.07 mL	0.59 mmol
THF	15 mL	

18 h at RT

Column 2:1:1 toluene: EtOAc: DCM R_f 0.72

Yield 57 mg (10 %)

Cr 118 °C Sm 144 °C N 147 °C I

M/Z Calculated mass [M+H]: 1120.6356 (C₇₉H₈₂N₃O₃) Found 1120.6350. Difference -0.5 ppm.

M/Z Calculated mass [M+Na]: 1142.6176 (C₇₉H₈₁N₃O₃Na) Found 1142.6177. Difference 0.1 ppm.

ν_{max}/cm^{-1} : 2925 (CH₂), 2854 (CH₂), 2226 (CN), 1635 (C=O), 1604 (Ar), 1004 (Ar), 812 (Ar).

^1H NMR (400 MHz, Chloroform-*d*) δ 7.66 (overlapping doublets, 8H, Ar-H), 7.62 (d, J = 8.3 Hz, 4H, Ar-H), 7.58 (d, J = 8.2 Hz, 4H, Ar-H), 7.48 (overlapping doublets, 4H, Ar-H) 7.20 (overlapping signals, 11H, Ar-H) 6.72 (d, J = 8.5 Hz, 1H, Ar-H), 6.53 (d, J = 8.4 Hz, 2H, Ar-H), 6.49 (d, J = 8.5 Hz, 1H, Ar-H), 6.45 (s, 1H, Ar-H), 5.19 (d, J = 13.9 Hz, 1H, N-CH), 4.56 (d, J = 13.9 Hz, 1H, N-CH), 3.77 (overlapping triplets, 4H, O-CH₂), 2.57 (overlapping triplets, 4H, Ar-CH₂), 1.74 (s, 3H, Ar-CH₃), 1.69 – 1.52 (m, 8H, CH₂-CH₂), 1.40 – 1.19 (m, 24H, CH₂-CH₂-CH₂).

^{13}C NMR (101 MHz, Chloroform-*d*) δ 169.95, 160.02, 157.97, 145.21, 145.18, 142.67, 142.66, 141.52, 141.50, 137.64, 137.62, 137.49, 137.47, 137.38, 136.74, 134.93, 132.64 (4C), 130.54 (2C), 130.13 (2C), 129.45 (2C), 128.98 (4C), 128.25, 128.13, 127.60 (4C), 127.56 (4C), 127.52 (4C), 127.35, 126.90 (4C), 118.98 (2C), 116.44, 113.22 (2C), 112.43, 110.86, 110.85, 68.00, 67.89, 53.70, 35.65, 35.64, 31.50, 31.47, 29.56, 29.53 (3C), 29.49 (2C), 29.41, 29.39, 29.36, 29.34, 29.28, 29.16, 26.05, 25.99, 18.01.

Supplementary Figures

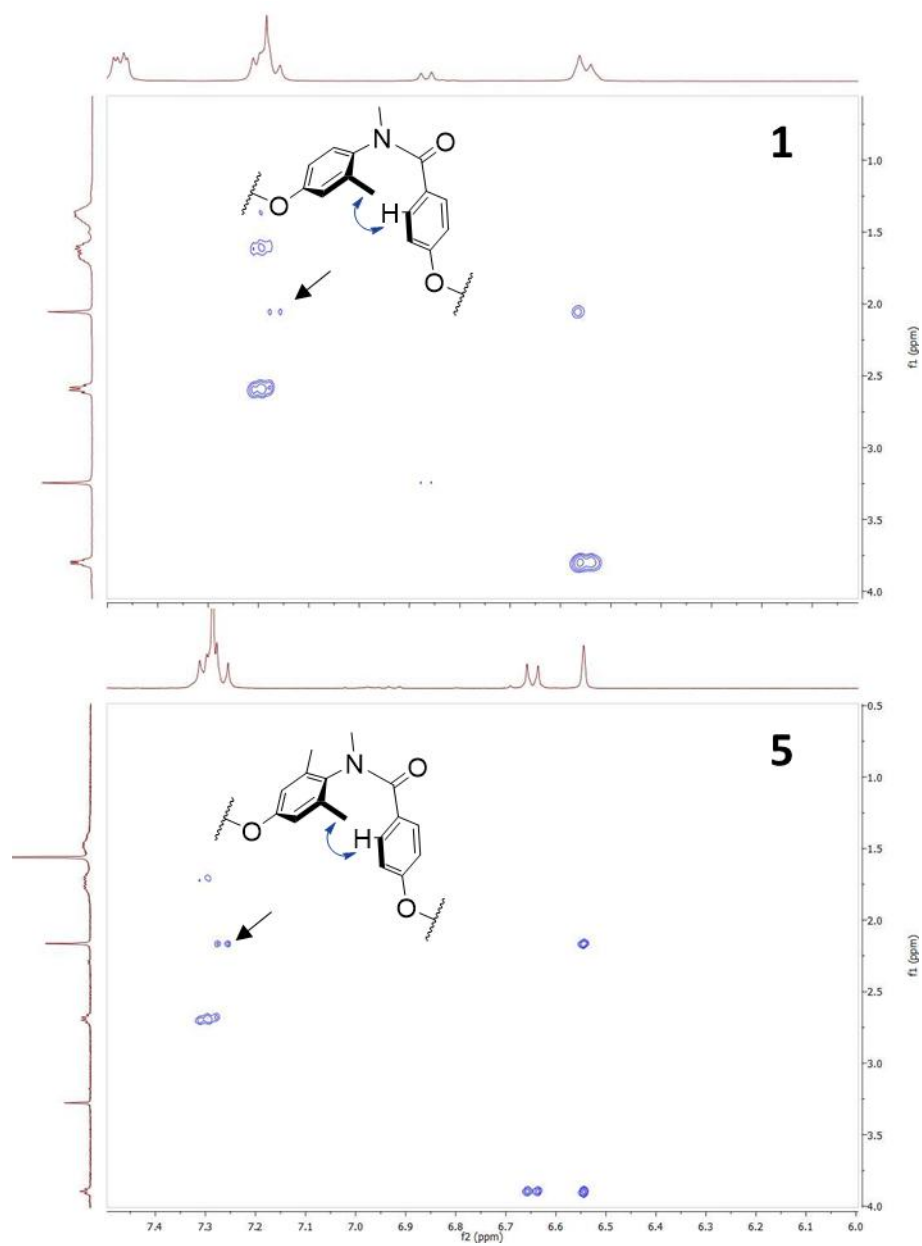


Figure S1: 2D NOESY spectra of trimer **1** (top) and **5** (below) showing cross-peaks between the aryl methyl and the protons ortho to the carbonyl.

Supplementary Information

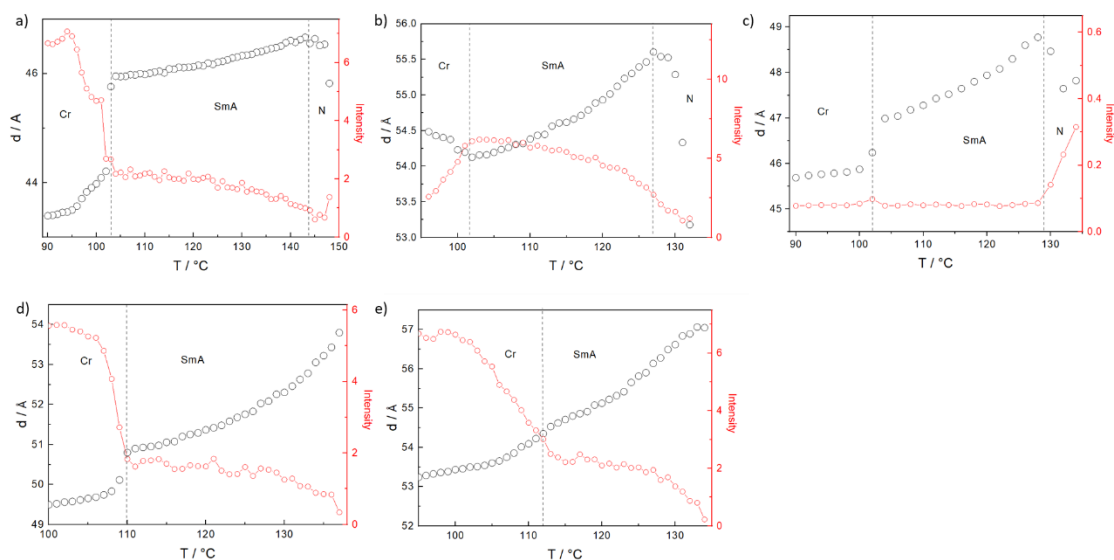


Figure S2: The temperature dependence of the layer spacing of trimer **2** (a), **8** (b), **9** (c), **10** (d), and **11** (e).

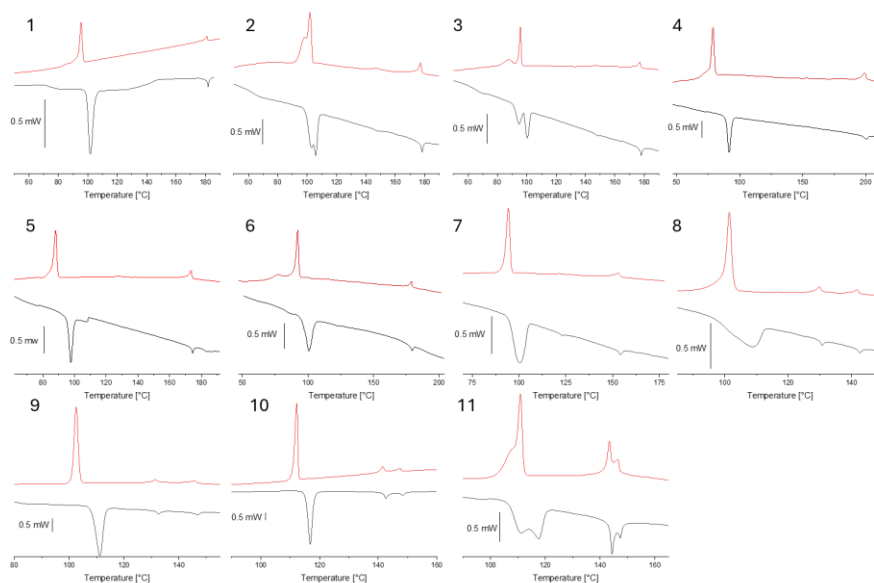


Figure S3: DSC traces for the new tertiary amide-based trimers.

References

- Strachan, G. J., Majewska, M. M., Pocięcha, D., Gorecka, E., Storey, J. M. D., & Imrie, C. T. (2024). Liquid crystal trimers containing secondary amide groups. *Liquid Crystals*. <https://doi.org/10.1080/02678292.2024.2382301>